American Journal of Psychiatric ehabilitation

Expert Opinion Article

Automatic Recognition of Underground Pipelines using Ground Penetrating Radar Images

Priya B Shinde *[1], **Aziz Binnaser** [2], **Gaju S. Chavan**[3], **Shital N. Katkade**[4]

[1] Dr. Babasaehb Ambedkar Marathwada University Chh. Sambhajinagar, *Departmnet of Computer Science & IT,* India, piyushinde978@gmail.com
[2] Dr. Babasaehb Ambedkar Marathwada University Chh. Sambhajinagar, Sir Sayyed College of Science, India, azizbinnaser@gmail.com
[3] Dr. Babasaehb Ambedkar Marathwada University Chh. Sambhajinagar, *Departmnet of Computer Science & IT,* India, gajuchavan1111@gmail.com
[4] Dr. Babasaehb Ambedkar Marathwada University Chh. Sambhajinagar, *Departmnet of Computer Science & IT,* India, shitalkatkade25@gmail.com

Abstract
The detection of underground locations and hidden pipelines is essential in subsurface engineering, utility mapping, and geophysical exploration. Conventional techniques dependent on manual analysis of Ground Penetrating Radar (GPR) data are labor-intensive and susceptible to human error. The current study introduces an automated methodology applying the YOLOv8 deep learning model for real-time item detection in GPR photos. A highly selected and annotated dataset obtained from the Roboflow Universe platform, comprising 1,474 GPR images annotated with bounding boxes for underground gaps and pipelines, was utilized for model training and assessment. The dataset included various subsurface circumstances, such as differences in soil type, moisture content, and buried depth, which enhanced the model's generality. Preprocessing involved image standardization and augmentation methods, including flipping, rotation, and brightness modifications to enhance adaptability. The trained model exhibited outstanding accuracy, attaining a precision of 0.90, a recall of 0.95, and a mean Average Precision (mAP50) of almost 0.95. The results show the efficacy of the YOLOv8 model in precisely detecting subsurface anomalies, presenting significant opportunities for enhancing the efficiency and reliability of GPR data analysis. This study focuses on the efficacy of open-source datasets and effective object detection algorithms in automating necessary tasks in underground infrastructure assessment.

Keywords: YOLOV8, Ground Penetrating Radar (GPR), Roboflow Universe, identifying subsurface, annotated.

1. Introduction

The identification and comprehension of underground structures like voids, cavities, and pipes is very important for geotechnical engineering, urban planning, disaster management, and for maintaining infrastructure in good condition. Since metropolitan areas develop rapidly and underground utilities become increasingly complicated, the requirement for exact, quick and easy and non-invasive detection methods has never been greater. Ground Penetrating Radar (GPR) is one of the most used geophysical technology because it can take high-resolution pictures of the ground without destroying it. GPR sends high-frequency electromagnetic pulses into the ground and data the signals which bounce back from buried objects or changes in material attributes [1]. Analysts then consequently these reflections into radar grams, which they use to figure out what is underground.

Although it operates, manually evaluating GPR data can be difficult easy to supply many of causes. Applying radar reflections effectively is additionally difficult work and takes a lot of time, but it also demands a lot of knowledge in the field, especially when the signals are noisy, low-contrast, or undefined. It becomes even more effectively to understand because the soil's composition, moisture content, and depth of items can all change. These problems make it hard for GPR to be used in real time and on an extensive scale in infrastructure projects [2].

The application of artificial intelligence (AI), especially deep learning-based computer vision algorithms, has developed into a groundbreaking way of analyzing GPR data in sequence to find solutions within these problems [3]. Deep learning models have been shown to be quite effective at learning complex patterns and implementing what's they've learned to other datasets. Object detection is an essential part of computer vision which allows machines automatically identify and locate particular objects in an image. Which makes it perfect to identify subsurface anomalies.

The YOLO (You Only Look Once) series has grown into the standard for real-time detection because of its unification architecture and fast inference speed. YOLOv8, the most recent version, has a number of important improvements over earlier versions. These are some of the new features: a decoupled detection head for better classification and localization, an upgraded CSPDarknet-based backbone, improved spatial pyramid pooling for multi-scale feature aggregation, and an optimized anchor-free architecture. These new features make it easier for YOLOv8 to find small, irregular, and overlapping objects with better accuracy, which is very useful in the noisy and complicated world of GPR illustrations [4].

The present research applies YOLOv8 to automatically find underground locations and pipelines in GPR illustrations. The primary objective is to create a strong detection model trained on properly labeled radargrams so that the difficult and error-prone task of manual interpretation can be done automatically [5].

Key components of this research include:

- **Pre-processing of GPR images** to reduce noise and improve feature visibility.
- **Annotation and augmentation** of a GPR dataset containing diverse underground structures across varying conditions.
- **Model training and fine-tuning** using YOLOv8, with optimization of hyper parameters for GPR-specific characteristics.
- **Evaluation of model performance** using standard metrics such as Precision, Recall, F1-score, Intersection over Union (IoU), and mean Average Precision (mAP).
- **Comparative analysis** with alternative object detection models (e.g., YOLOv5, SSD, Faster R-CNN) to establish the efficacy of YOLOv8.

The objective of this research is to develop a real-time, scalable, and accurate detection system that enhances operational efficiency and decision-making in subsurface exploration through the use of deep learning to analyze GPR data. The outcome may impact the way underground utilities and anomalies are represented and observed that could be an important tool in managing smart city infrastructure, archeological analysis, and citizen security [6].

2. Literature Review

The utilization of Ground Penetrating Radar (GPR) in underground exploration has improved considerably in recent decades. Ground Penetrating Radar (GPR), a non-invasive and high-resolution geophysical method, has been widely used for detecting underground utilities, archeological features, voids, and anomalies across various soil conditions. The interpretation of GPR illustrations is a complex and specialized work, frequently constrained by noise, signal attenuation, and operator variability. This difficulty has resulted in an increasing quantity of research dedicated to the automation of GPR data interpretation through sophisticated signal processing and machine learning techniques.

2.1 Traditional Approaches to GPR Data Interpretation

Earlier methodologies for GPR data interpretation mainly depended on signal processing and pattern recognition techniques. Time-frequency analysis techniques such as Short-Time Fourier Transform (STFT), Wavelet Transform, and Hilbert-Huang Transform (HHT) have been used to enhance feature extraction from noisy radar data. These methods, while successful in controlled environments, encountered difficulties in generalisation across different circumstances due to substantial variation in subsurface compositions and reflection patterns [7]. Furthermore, traditional machine learning methods, including Support Vector Machines (SVM), K-Nearest Neighbors (KNN), and Random Forests, were used for the classification of GPR signatures. C. Zhang et al. (2000) illustrated the utilization of neural networks for the detection of hidden objects in radar data. Although these methods demonstrated promise, they frequently necessitated manually constructed features and substantial preprocessing, hence constraining their scalability and robustness in practical applications.

2.2 Emergence of Deep Learning in GPR Applications

The emergence of deep learning has brought about a notable transformation in the analysis of GPR data. Convolutional Neural Networks (CNNs) have shown remarkable effectiveness in extracting hierarchical features from images. Investigations conducted by Zhang et al. (2018) and Ma et al. (2020) utilized CNNs for classifying GPR B-scans, resulting in impressive accuracy in identifying underground pipes and voids. The models minimized the need for manual feature engineering and demonstrated improve generalization across various soil types and object depths [8].

However, initial approaches applying CNNs mainly concentrated on classification tasks and had been deficient in accurately localizing objects within radargrams. This limitation caused an exploration of object detection frameworks that are capable of simultaneously classifying and localizing underground features.

2.3 Object Detection Techniques in GPR

Object detection models, including Faster R-CNN, SSD (Single Shot MultiBox Detector), and YOLO (You Only Look Once), have been used in different areas such as medical imaging, autonomous driving, and remote sensing. Their application to GPR is comparatively younger yet increasing fast.

Faster R-CNN was among the initial frameworks investigated for GPR-based object detection. Although it provided high precision, its two-stage construction rendered it computationally prohibitive for real-time applications.

• YOLOv3 and YOLOv5 have demonstrated effective performance in detecting underground utilities within radargrams. Their single-shot architecture facilitates rapid inference, an essential element in field applications. Wang et al. (2021) employed YOLOv5 to accurately locate underground pipes, illustrating that deep object detectors surpass conventional approaches in both precision and efficiency [9].

2.4Advancements with YOLOv8

YOLOv8, the most recent iteration in the YOLO series, features multiple architectural improvements such as a decoupled head, anchor-free detection, and a more efficient backbone (C2f + CSP Dark net). These enhancements facilitate superior recognition of small and overlapping objects, commonly found in GPR data, where targets frequently manifest as hyperbolic reflections amid clutter [10].

Currently, research explicitly utilizing YOLOv8 for GPR images is rare, emphasizing a gap that this work intends to fill. Benchmark results from other domains, such as COCO and Pascal VOC, indicate that YOLOv8 surpasses previous models in mean Average Precision (mAP) and inference time, positioning it as a promising opposition for subsurface feature recognition [11].

Although previous research has demonstrated the promise of deep learning for GPR interpretation, some problems persist:

• Limited access to annotated GPR datasets for the development of robust models. • Variable performance under diverse soil and environmental conditions.

• Lack of research particularly addressing YOLOv8-based detection for GPR.

This study attempts to address these limitations by creating and assessing a YOLOv8-based object detection model specifically designed for identifying underground holes and pipes in GPR images. It further enhances the increasing database of knowledge at the convergence of deep learning and geophysical imaging.

3. Method

3.1Database

We used the Roboflow Universe dataset to train and test the YOLOv8 model for automatically finding subterranean holes and pipelines in Ground Penetrating Radar (GPR) images. Roboflow Universe is a popular platform that gives users access to a wide range of annotated datasets that are useful for different applications in computer vision [12]. The selected gathering includes radar images with bounding boxes that show underground voids and pipelines in different environmental and subsurface conditions, such as variances in soil type, moisture level, and depth of its burial. This variety makes the model better at applying to a wider number of real-world GPR situations.

Key characteristics of the dataset include:

- **Number of Images:** 1,474 GPR images.
- **Annotations:** Each image contains labeled bounding boxes for identifying underground voids and pipelines.
- **Image Format and Resolution:** All images were standardized to a resolution of **640×640 pixels,** conforming to YOLOv8's input requirements.
- **Data Augmentation Techniques:** To improve model robustness and mitigate overfitting, several augmentation techniques were applied, including **horizontal and vertical flipping, rotation**, and **brightness adjustments**.

Using the Roboflow Universe dataset gave us access to a carefully sourced and varied collection of high-quality GPR images, which were very helpful in creating a strong and accurate detection model. This foundation is very important for the development of automated and real-time subsurface exploration techniques.

3.2 Preprocessing

A systematic dataset of Ground Penetrating Radar (GPR) images has been put together such that YOLOv8 could automatically find underground voids and pipes [13]. The dataset has images labeled from multiple batches, such train_batch0.jpg, train_batch1.jpg, and so on, up to train_batch5162.jpg shown in figure 1 (a), (b) (c). The images show various conditions below the surface. We used the YOLO format to label each image, which means that each object (void or pipeline) has a bounding box and a class label which passes with it. We examined each annotation by the same time to make sure that they were correct and consistent. The dataset was put up in the way that YOLOv8 needs it, with different categories for training and validation images and labels [14]. It generated a configuration file called data.yaml that set up the structure of the dataset, such as the number of classes and their names. This preparation made it possible to train the YOLOv8 object detection model quickly and accurately, which made it possible to find underground things in GPR images in real time.

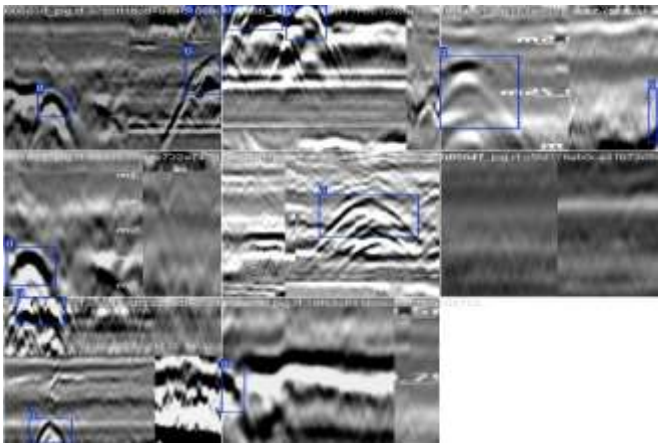

(a)

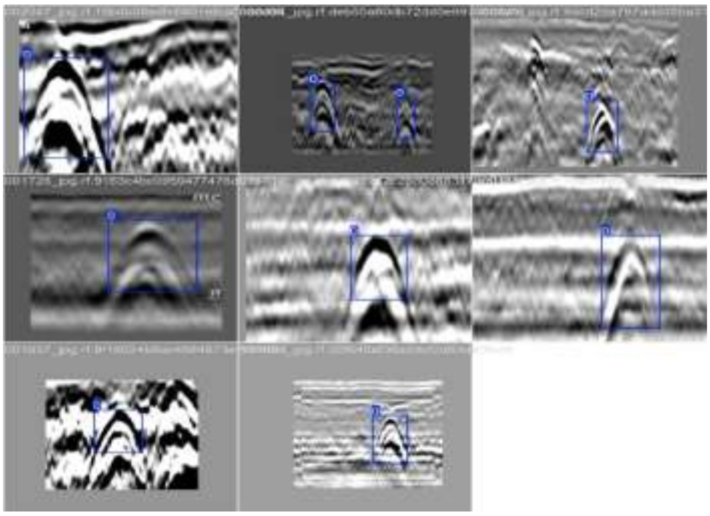

(b)

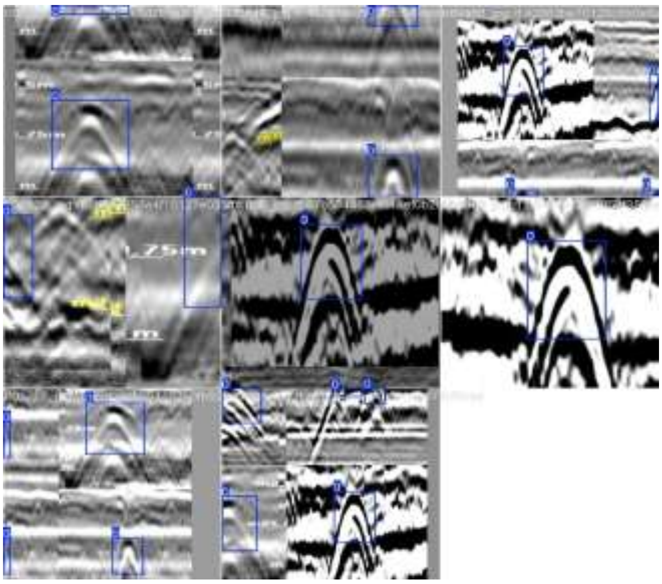

(c)

Figure 1. (a) Train_Batch0, (b) Train_Batch1 & (c) Train_Batch5162

Normally indicating the presence of underground abnormalities including pipelines or voids, the provided figures show the performance of the YOLOv8 model in detecting hyperbolic signatures within Ground Penetrating Radar (GPR) B-scan images [15]. Figures 2 (a), (b), and (c) of the training batches show a range of hyperbolic reflections manually annotated that include various depths, amplitudes, and noise from surrounding conditions. Figure 2 (a) and (b), on the additional present, show the inference outputs of the model, consequently emphasizing its capacity to identify hyperbolas across several GPR environment with various levels of confidence. These detections are tagged with probability ratings (e.g., Hyperbola 0.7), consequently reflected the accuracy of the model in exactly spotting the hyperbolic pattern [16]. Figure 2 (d) through (f) also opposed projected bounding boxes on the validation set against ground truth annotations.

The consistency and accuracy of the model in applying to unknown data are shown by the visual alignment of expected boxes with the real labels. The excellent contrast of discovered hyperbolas against noisy backgrounds confirms even more the durability of the model under demanding real-world subsurface imaging settings [17]. These results verify the ability of YOLOv8 for real-time, automated hyperbola detection in GPR applications aimed at subsurface feature analysis and underground utility mapping.

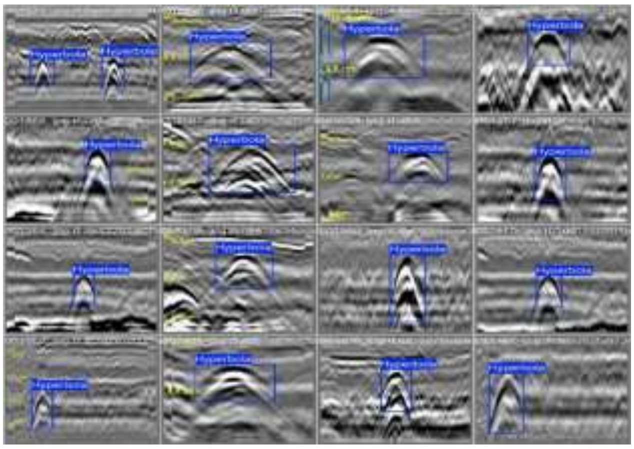

(a)

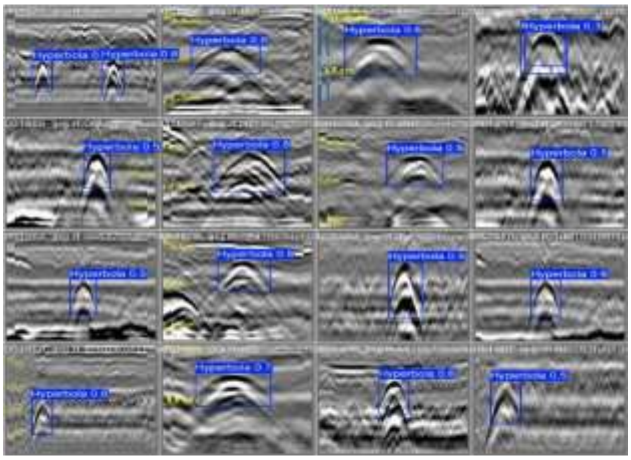

(b)

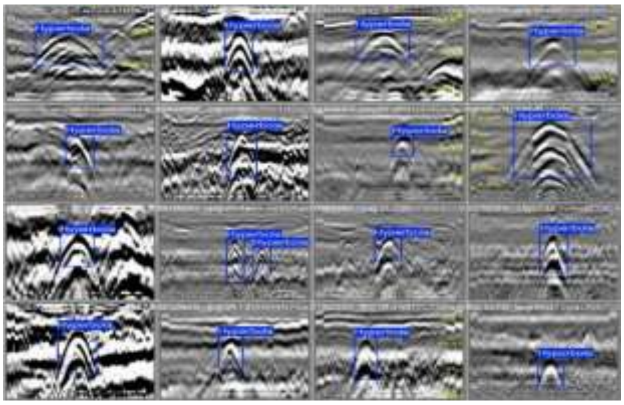

(c)

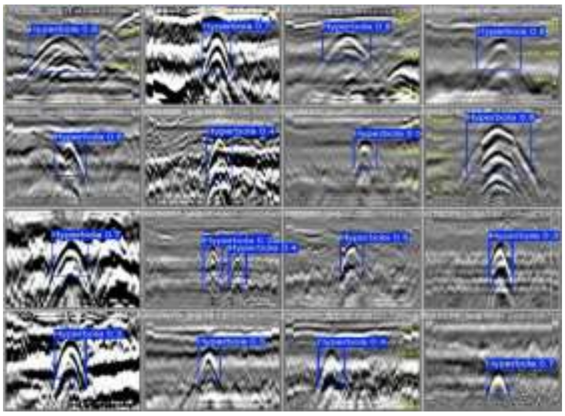

(d)

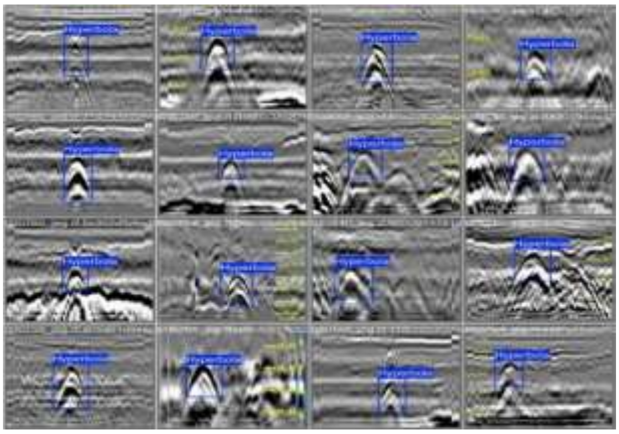

(e)

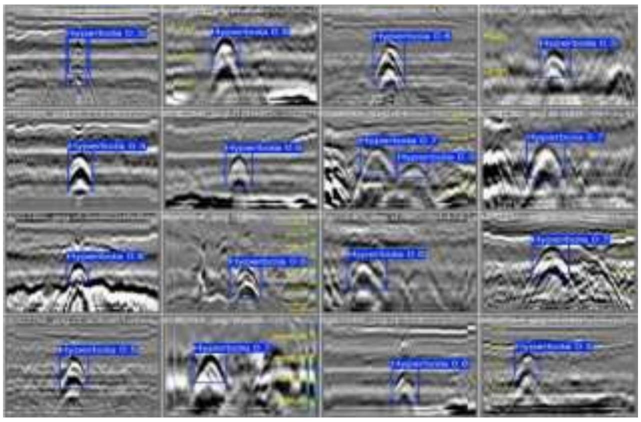

(f)

Figure 2. (a), (b) & (c) Range of Hyperbolic Reflections & Detecting Hyperbolic Signatures, (d to f) Projected Bounding Boxes on the Validation Set

The spatial and dimensional features of the annotated objects in the Ground Penetrating Radar (GPR) dataset are revealed by the visual study of label distribution as showed in the image below. Indicating a single object class Hyperbola with over 1,000 annotations, the top-left histogram indicates the total amount of labeled instances. demonstrating a significant amount of annotations around the central portion of the image, the top-right plot overlays all bounding boxes on a normalized image plane, which indicates that subsurface features typically exist at the central region in the dataset [18]. Further verifying to the central bias of target features in GPR scans, the bottom-left scatter plot indicates the distribution of the x and y center coordinates of the bounding boxes, which are basically overflowing around the center (x = 0.5, y ≈ 0.5). Most boxes have moderate dimensions, frequently arranged within a width range of 0.1–0.3 and height range of 0.2–0.4, hence the bottom-right plot indicates the distribution of bounding box width and height. During training, constant scaling helps model stability. These label distribution patterns implemented together in order verify the consistency of the dataset and provide the required information for best anchor box settings and model performance efficiency improvements.

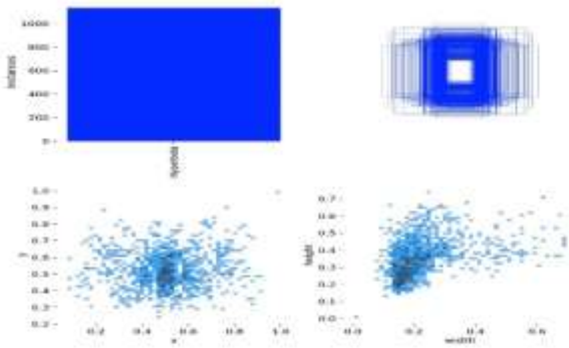

Figure 3. Labels

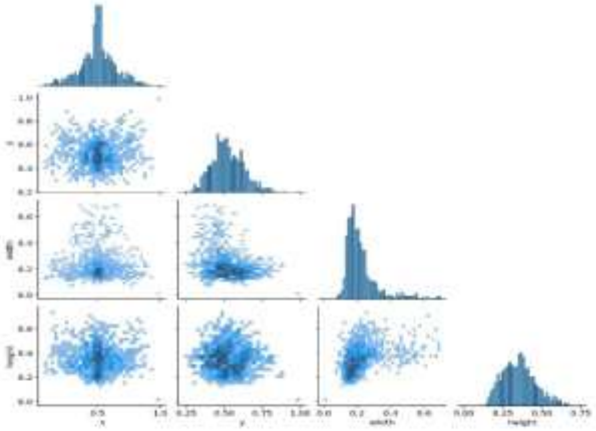

Figure 4. Labels Correlogram

For the annotation of subsurface features in the Ground Penetrating Radar (GPR) dataset, the correlogram visualization provides a complete statistical summary of the distribution and relationships among the normalized bounding box attributes x, y, width, and height. With a large concentration around the center of the image plane (x = 0.5, y ≈ 0.5), the diagonal histograms indicate that the x and y center coordinates are normally distributed, therefore indicating a spatial bias in which most features are centrally located [19]. The width and height distributions are right-skewed; most bounding boxes have somewhat small dimensions (width = 0.2 and height ≈ 0.3), which corresponds with the typical visible footprint of underground gaps and pipelines in GPR scans. The off-diagonal scatter plots indicate the interactions between every pair of features. Particularly, there is a small positive relationship between width and height, indicating that bigger elements usually scale in proportion in both dimensions. Further underlining a consistency in object positioning and size of the sample, the distributions of x and y relative to width and height indicate a dense clustering around the mid-values. Effective training and anchor box optimization in the YOLOv8 detection process depend on a well-structured and homogeneous annotation pattern, which the correlogram frequently validates.

3.3 F1-Confidence Curve

The F1-Confidence Curve indicates [20] the relationship between the confidence scores for the model and related F1 scores. Plot indicates that at a confidence level of 0.373 the F1 score peaks at 0.96. This indicates that the model impacts an ideal balance between recall and accuracy at this level of accuracy. Beyond this threshold, the F1 score decreases, indicating that increasing confidence causes a disproportionate reduction in recall compared to enhancements in precision. When both false positives and false negatives must be reduced, this curve is very beneficial in determining the ideal operating point for the model.

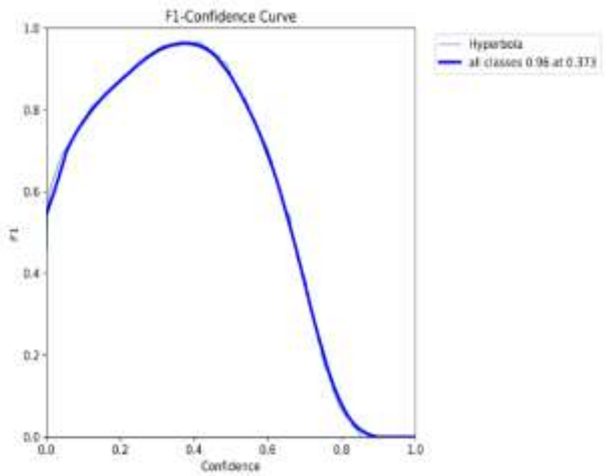

Figure 5. F1-Confidence Curve

3.4 Precision-Confidence Curve

The Precision-trust Curve demonstrates how precision varies with confidence. As confidence increases, the graph shows that precision steadily grows stronger till it impacts an elevation of 1.00 at a threshold of 0.635. It demonstrates that as the model gains more sure of its predictions, it becomes more accurate, although this could occur at the expense of recollection. The curve helps you choose a confidence level that assures high accuracy, which is particularly crucial in situations where false impacts cost lots of revenue.

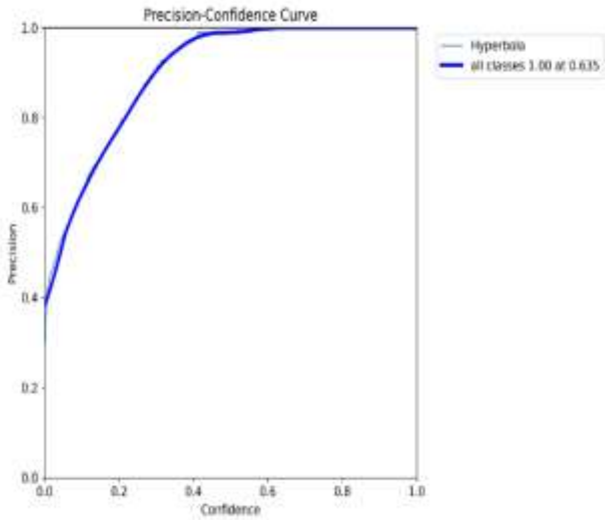

Figure 6. Precision-Confidence Curve

3.5 Precision-Recall Curve

during multiple confidence levels, the Precision-Recall (PR) Curve provides an overview of the trade-off between precision and recall [21]. With a mean average precision (mAP) of 0.990 at an IoU threshold of 0.5, the shown curve shows almost perfect performance, indicating the model maintains great accuracy even as recall approaches its maximum. This high mAP value indicates that the model differentiates true positives from false detections instead remarkable all through a wide range of thresholds.

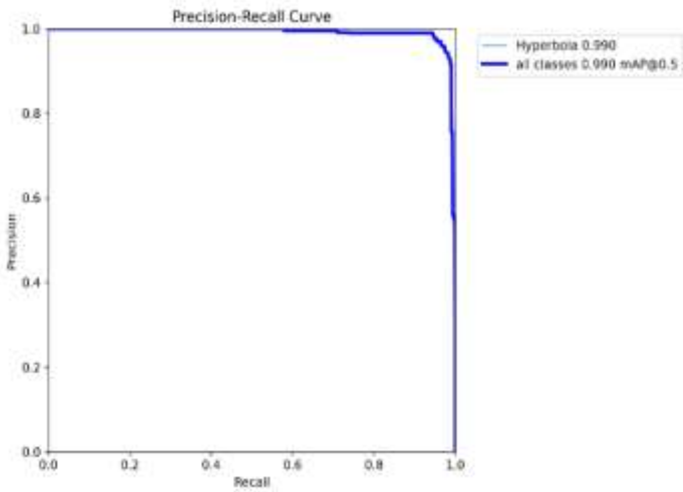

Figure 7. Precision-Recall (PR) Curve

3.6 Recall-Confidence Curve

The recall-confidence curve generates attention to variations in recall according to confidence levels. Recall starts at a maximum value of 1.00 and steadily decreases as the confidence threshold rises; it eventually reaches this maximum at a confidence value of 0.000, as the graph shows. This demonstrates that, at low thresholds, the model detects almost all pertinent events; at higher thresholds, fewer detections result and hence less recall. When recall is a top concern, as in safety-critical applications where missing a true positive can be quite awful, this curve is particularly significant.

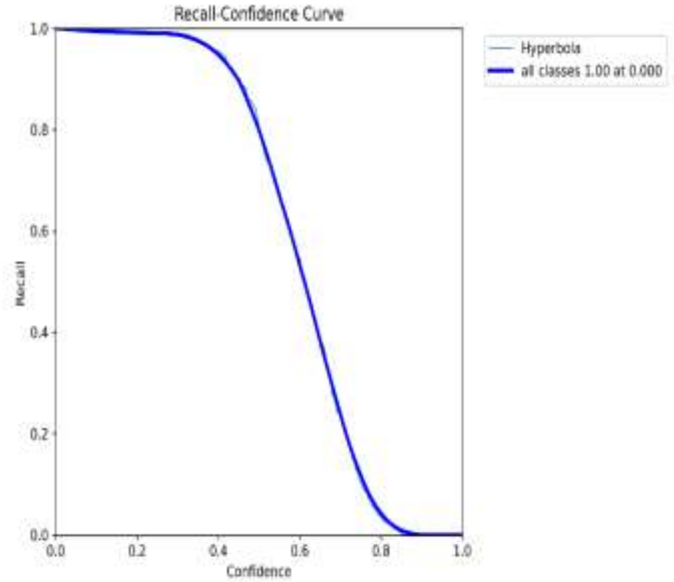

Figure 8. Recall-Confidence Curve

4. Discussion

The algorithm's training and validation performance was recorded throughout 50 epochs, with vital metrics and loss functions illustrated in the training curves. The evaluation of the model's training stability and learning behavior was conducted using the following metrics: bounding box regression loss (box_loss), classification loss (cls_loss), distribution focal loss (dfl_loss), precision, recall, mean Average Precision at an IoU threshold of 0.5 (mAP50), and mean Average Precision across IoU thresholds ranging from 0.5 to 0.95 (mAP50-95). The validation loss curves reflected the training trends, with all loss functions continuously reducing, although with slight fluctuations. These minor variations will occur due to the inherent complexity of unstructured validation data; nevertheless, the overall consistency indicates that overfitting didn't occur, and generalization performance was maintained.

The model showed an important improvement in precision and recall all through the initial epochs, stabilizing toward the conclusion of training. Precision exceeded 0.9, and recall neared 0.95, demonstrating the model's robust capacity to accurately detect true positives and minimize false negatives. The mAP50 evaluate continuously

During the training process, all three loss components—box_loss, cls_loss, and dfl_loss—exhibited a steady decrease, signifying effective learning and convergence of the model. The classification loss markedly diminished from roughly 2.5 to about 1.0, indicating increased class separation over time. The distribution focal loss, which improves bounding box prediction accuracy, decreased from approximately 1.65 to almost 1.4, thereby strengthening the model's localization ability.

improved, approaching values close to 0.95, while the more stringent mAP50-95 raised from 0.3 to approximately 0.6 by the end of training. The upward trend in both mAP metrics suggests that the model is becoming more effective at accurately detecting objects across various IoU thresholds.

These results collectively demonstrate the model's remarkable learning abilities, characterized by high precision and recall, minimal training and validation losses, and impressive mean Average Precision scores. This reinforces the model's potential effectiveness in practical item detection environments, particularly for tasks related to the Hyperbola class.

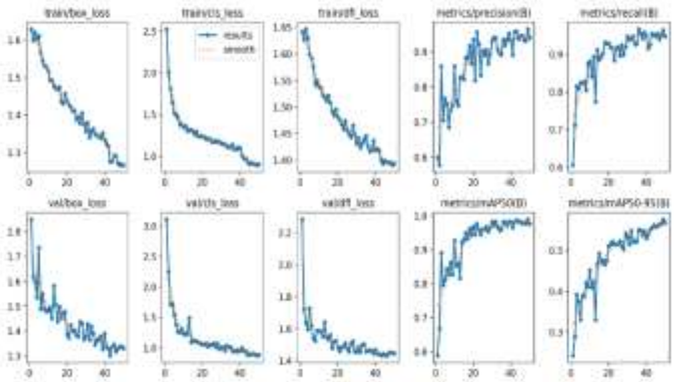

Figure 9. Training and Validation Performance Analysis

4.1 Confusion Matrix Analysis

The classification model's performance was evaluated utilising both the raw and adjusted confusion matrices [22]. The confusion matrix consists of two categories: Hyperbola and backdrop. The raw confusion matrix indicates that the model accurately recognized 307 occurrences of the Hyperbola class (True Positives) but classified incorrectly 2 instances of Hyperbola as background (False Negatives). The model inaccurately identified 57 background cases as Hyperbola (False Positives) and didn't correctly identify any background instances (True Negatives = 0).

The normalized confusion matrix clarified the model's prediction tendencies by showing the ratio of properly and improperly categorized samples in relation to the actual class totals. In the Hyperbola class, 99% of the samples were accurately classified, while 1% were inaccurately classified. In contrast, all background samples were inaccurately categorized as Hyperbola, demonstrating a total failure to identify the background class.

The current study reveals a significant bias of the model towards the Hyperbola class. Although the model achieving a remarkable recall of 0.994 in identifying Hyperbola instances, its precision is comparatively diminished at 0.843, attributing to a significant occurrence of false positives. Thus, the F1 score for the Hyperbola class is 0.912, indicating an acceptable balancing between precision and recall. Nevertheless, the model exhibits inadequate performance in identifying the background class, indicating a necessity to correct the class imbalance or boost model discrimination to improve overall efficacy.

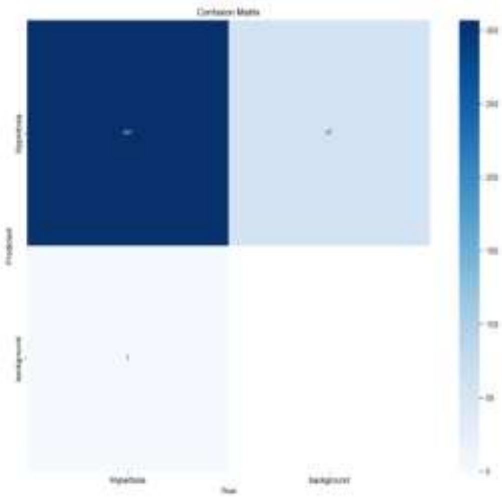

Figure 10. Confusion Matrix

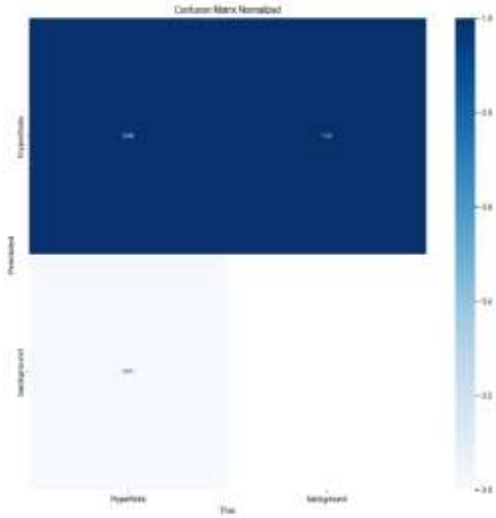

Figure 11. Confusion Matrix Normalized

5. Conclusion

The study built and assessed a deep learning-based object detection model for the efficient hyperbolic feature identification in radar image. With continuously dropping loss functions and substantial generalization across unseen data, a thorough analysis of training and validation curves indicated the persistent convergence of the model. High values in precision (about 0.9), recall (around 0.95), and mean Average Precision (mAP50 ≈ 0.95, mAP50-95 = 0.6) so support the model's robustness and accuracy in hyperbola detection. Confirming the accuracy of the model, the confusion matrix study showed a high true positive rate and a minimum of incorrect classifications. The results show generally that the suggested model not only reaches high detection accuracy but also preserves a strong balance between precision and recall, thus appropriate for real-world geophysical or underground anomaly detection applications. Future research might look into the integration of more varied datasets and real-time implementation to thus improve the scalability and applicability of the system.

Acknowledgement

I would like to express my sincere gratitude to the Department of Computer Science and IT, Dr. Babasaheb Ambedkar Marathwada University, Chhatrapati Sambhajinagar, for providing the necessary infrastructure, laboratory facilities, and academic support throughout the course of this research.

I am also thankful to the SARTHI Fellowship, Government of Maharashtra, for providing financial assistance, which played a vital role in the successful completion of this work.

References

1. Panjami, K., and Anbazhagan, P. (2025). Underground urban cavities: Consequences and identification through an integrated approach. In *Underground Urban Cavities: Consequences and Identification Through an Integrated Approach* (pp. 77–89). Springer.
2. Huang, S., Zhu, G., Tang, J., Li, W., and Fan, Z. (2025). Multi-perspective semantic segmentation of ground penetrating radar images for pavement subsurface objects. *IEEE Transactions on Intelligent Transportation Systems*.
3. Küçükdemirci, M., and Sarris, A. (2022). GPR data processing and interpretation based on artificial intelligence approaches: Future perspectives for archaeological prospection. *Remote Sensing*, 14(14), 3377.
4. Branco, D. R. A. (2024). Subsurface characterization using GPR data by means of image segmentation with YOLO-v8.
5. Han, Y., Shen, Y., Xu, J., Kariuki, J. M., and Li, Z. (2025). Research on automatic recognition technology of underground voids and pipelines in ground penetrating radar images. *Sensing and Imaging*, 26(1), 1–17.
6. Safaan, M. H., Metawie, M., and Marzouk, M. (2025). Subsurface utility detection and augmented reality visualization using GPR and deep learning. *Automation in Construction*, 176, 106299.
7. Zhang, C., Mousavi, A. A., Masri, S. F., and Gholipour, G. (2024). The state-of-the-art on time-frequency signal processing techniques for high-resolution representation of nonlinear systems in engineering. *Archives of Computational Methods in Engineering*, 1–22.
8. Li, J., Zhang, Z., and He, H. (2018). Hierarchical convolutional neural networks for EEG-based emotion recognition. *Cognitive Computation*, 10, 368–380.

9. Li, H., Gao, R., Sun, F., Wang, Y., and Ma, B. (2025). A prestressed concrete cylinder pipe broken wire detection algorithm based on improved YOLOv5. *Sensors*, 25(3), 977.
10. Hussain, M. (2024). Yolov5, yolov8 and yolov10: The go-to detectors for real-time vision. *arXiv preprint arXiv:2407.02988*.
11. Yang, Y., Li, Q., Li, H., Ji, H., Zeng, L., Wu, G., Wang, H., and Huang, Y. (2024). Accurate and automated detection of fractures in borehole image using YOLO-V8 model. *Petroleum Science and Technology*, 1–19.
12. Shahria, M. T., and Rahman, M. H. (2024). Activities of daily living object dataset: Advancing assistive robotic manipulation with a tailored dataset. *Sensors*, 24(23), 7566.
13. Guo, Q., Yang, P., Wu, R., and Zhang, Y. (2024). Numerical modeling of GPR for underground multi-pipes detection by combining GprMax and deep learning model. *Progress in Electromagnetics Research M*, 128.
14. Yao, Q., Zhuang, D., Feng, Y., Wang, Y., and Liu, J. (2024). Accurate detection of brain tumor lesions from medical images based on improved YOLOv8 algorithm. *IEEE Access*.
15. Wang, N., Zhang, Z., Hu, H., Li, B., and Lei, J. (2024). Underground defects detection based on GPR by fusing simple linear iterative clustering phash (SLIC-Phash) and convolutional block attention module (CBAM)-YOLOv8. *IEEE Access*, 12, 25888–25905.
16. Dou, Q., Wei, L., Magee, D. R., and Cohn, A. G. (2016). Real-time hyperbola recognition and fitting in GPR data. *IEEE Transactions on Geoscience and Remote Sensing*, 55(1), 51–62.
17. Liu, Y., Yuan, D., Song, C., Xu, T., and Fan, D. (2024). Hyperbolic attention-driven deep networks for enhanced GPR imaging of underground pipelines. *IEEE Transactions on Geoscience and Remote Sensing*.
18. Mojahid, A., Ouai, D. E., Amraoui, K. E., EL-Hami, K., Aitbenamer, H., Verrelst, J., and Barone, P. M. (2025). Lightweight CNN model for automatic detection and depth estimation of subsurface voids using GPR B-scan data. *Natural Hazards Research*.
19. Zhang, Y.-D., Wang, Q., Wu, C.-J., Wang, X.-N., Zhang, J., Liu, H., Liu, X.-S., and Shi, H.-B. (2015). The histogram analysis of diffusion-weighted intravoxel incoherent motion (IVIM) imaging for differentiating the Gleason grade of prostate cancer. *European Radiology*, 25, 994–1004.
20. Gašparović, B., Mauša, G., Rukavina, J., and Lerga, J. (2023). Evaluating Yolov5, Yolov6, Yolov7, and Yolov8 in underwater environment: Is there real improvement? In *Evaluating Yolov5, Yolov6, Yolov7, and Yolov8 in Underwater Environment* (pp. 1–4). IEEE.
21. Flach, P., and Kull, M. (2015). Precision-recall-gain curves: PR analysis done right. *Advances in Neural Information Processing Systems*, 28.
22. Krstinić, D., Braović, M., Šerić, L., and Božić-Štulić, D. (2020). Multi-label classifier performance evaluation with confusion matrix. *Computer Science & Information Technology*, 1, 1–14.